



Published in final edited form as:

Chem Sci. 2015 October 1; 6(10): 5670–5679. doi:10.1039/C5SC02102B.

## Protonation state of the Cu<sub>4</sub>S<sub>2</sub> Cu<sub>Z</sub> site in nitrous oxide reductase: redox dependence and insight into reactivity

Esther M. Johnston<sup>a</sup>, Simone Dell'Acqua<sup>b</sup>, Sofia R. Pauleta<sup>c</sup>, Isabel Moura<sup>c</sup>, and Edward I. Solomon<sup>a</sup>

<sup>a</sup>Department of Chemistry, Stanford University, Stanford, CA 94305

<sup>b</sup>Dipartimento di Chimica, Università di Pavia, Via Taramelli 12, 27100 Pavia, Italy

<sup>c</sup>UCIBIO, REQUIMTE, Departamento de Química, Faculdade de Ciências e Tecnologia, Universidade Nova de Lisboa, 2829-516 Caparica, Portugal

### Abstract

Spectroscopic and computational methods have been used to determine the protonation state of the edge sulfur ligand in the Cu<sub>4</sub>S<sub>2</sub> Cu<sub>Z</sub> form of the active site of nitrous oxide reductase (N<sub>2</sub>OR) in its 3Cu<sup>I</sup>Cu<sup>II</sup> (1-hole) and 2Cu<sup>I</sup>2Cu<sup>II</sup> (2-hole) redox states. The EPR, absorption, and MCD spectra of 1-hole Cu<sub>Z</sub> indicate that the unpaired spin in this site is evenly delocalized over Cu<sub>I</sub>, Cu<sub>II</sub>, and Cu<sub>IV</sub>. 1-hole Cu<sub>Z</sub> is shown to have a μ<sub>2</sub>-thiolate edge ligand from the observation of S-H bending modes in the resonance Raman spectrum at 450 and 492 cm<sup>-1</sup> that have significant deuterium isotope shifts (−137 cm<sup>-1</sup>) and are not perturbed up to pH 10. 2-hole Cu<sub>Z</sub> is characterized with absorption and resonance Raman spectroscopies as having two Cu-S stretching vibrations that profile differently. DFT models of the 1-hole and 2-hole Cu<sub>Z</sub> sites are correlated to these spectroscopic features to determine that 2-hole Cu<sub>Z</sub> has a μ<sub>2</sub>-sulfide edge ligand at neutral pH. The slow two electron (+1 proton) reduction of N<sub>2</sub>O by 1-hole Cu<sub>Z</sub> is discussed and the possibility of a reaction between 2-hole Cu<sub>Z</sub> and O<sub>2</sub> is considered.

### 1. Introduction

The main reductive part of the nitrogen cycle, known as bacterial denitrification, is performed by soil and marine bacteria as a means of anaerobic or microaerobic respiration. Denitrification involves the conversion of nitrate to dinitrogen via four successive reductive steps (NO<sub>3</sub><sup>-</sup> → NO<sub>2</sub><sup>-</sup> → NO → N<sub>2</sub>O → N<sub>2</sub>), each performed by a different metalloenzyme.<sup>1</sup> The terminal product of denitrification can be either N<sub>2</sub>O or N<sub>2</sub>, depending on the regulatory control of the N<sub>2</sub>O reduction process and whether the bacterium involved contains the gene cluster for nitrous oxide reduction (the *nos* cluster; *nosZ* encodes the nitrous oxide reductase enzyme).<sup>2,3</sup> The N<sub>2</sub>O reduction process and its regulation *in vivo*

No competing financial interests have been declared.

Electronic Supplementary Information (ESI) available: Full experimental and computational methodology, EPR quantification of the Cu<sub>Z</sub><sup>\*</sup>/Cu<sub>Z</sub> ratio, 2<sup>nd</sup> derivative of the X band EPR of 1-hole Cu<sub>Z</sub>, table of absorption band energies and assignments for 1-hole Cu<sub>Z</sub> and 1-hole Cu<sub>Z</sub><sup>\*</sup>, resonance Raman spectrum and profile of 1-hole Cu<sub>Z</sub><sup>\*</sup>, pH dependence of the spectral features of 1-hole and 2-hole Cu<sub>Z</sub>, low temperature absorption spectrum of 2-hole Cu<sub>Z</sub>, and computational structures, vibrations, and TD-DFT absorption spectra for models of 1-hole and 2-hole Cu<sub>Z</sub> (1-hole SH<sup>-</sup> and OH<sup>-</sup> and 2-hole SH<sup>-</sup> and S<sup>2-</sup> models). See DOI: 10.1039/b000000x/

are of significant interest because N<sub>2</sub>O is a potent greenhouse gas, with a global warming potential 300× that of CO<sub>2</sub>,<sup>4, 5</sup> and depletes the ozone layer.<sup>6</sup> Anthropogenic sources of environmental N<sub>2</sub>O, the majority of which is due to agricultural activity, is an increasing contribution to the global atmosphere.<sup>2</sup> Soil studies have indicated that pH,<sup>7, 8</sup> temperature,<sup>9</sup> acetylene,<sup>10</sup> sulfide,<sup>11</sup> and dioxygen<sup>12</sup> all affect the production of N<sub>2</sub>O, but the molecular basis of these effects is still not known. A molecular understanding of nitrous oxide reduction and how this process is regulated could enable mitigation of N<sub>2</sub>O release from anthropogenic sources.<sup>5</sup>

Nitrous oxide reductase contains two copper sites: a binuclear site known as Cu<sub>A</sub> that functions as an electron transfer site, and an unusual tetranuclear copper sulfide cluster active site, where N<sub>2</sub>O binds and is reduced (Figure 1). Two forms of this tetranuclear site have been structurally characterized. One, known as Cu<sub>Z</sub><sup>\*</sup>, has a μ<sub>4</sub> sulfide ligand bridging all four coppers and a solvent derived ligand on an open edge (the Cu<sub>I</sub>-Cu<sub>IV</sub> edge) where N<sub>2</sub>O is proposed to bind (Figure 1A).<sup>13</sup> This edge ligand has previously been assigned as a bridging hydroxide ligand, due to the presence of a vibration in the resonance Raman spectrum of Cu<sub>Z</sub><sup>\*</sup> that shifts in H<sub>2</sub><sup>18</sup>O solvent at high pH and the absence of significant spectroscopic differences between Cu<sub>Z</sub><sup>\*</sup> at high and low pH.<sup>15</sup> The other form of the cluster, known as Cu<sub>Z</sub>, has an additional μ<sub>2</sub> sulfur ligand bridging the Cu<sub>I</sub>-Cu<sub>IV</sub> edge (Figure 1B).<sup>14</sup> Whether the μ<sub>2</sub> edge ligand in Cu<sub>Z</sub> is a thiolate (SH<sup>-</sup>) or a sulfide (S<sup>2-</sup>) and how its protonation depends on the redox state of the cluster are not known. The Cu<sub>4</sub>S<sub>2</sub> Cu<sub>Z</sub> form of the cluster is dominantly isolated when N<sub>2</sub>OR is purified in the absence of oxygen<sup>16</sup> or rapidly in the presence of oxygen,<sup>17</sup> while the Cu<sub>4</sub>S Cu<sub>Z</sub><sup>\*</sup> form is isolated when the purification is performed aerobically or anaerobically from mutants in the accessory genes;<sup>16-18</sup> however, all purifications typically yield enzyme with a mixture of the two sites.<sup>17, 19</sup> Which structural form of the cluster is responsible for N<sub>2</sub>O reduction *in vivo* is a matter of some debate.<sup>20-22</sup> As isolated, neither N<sub>2</sub>OR containing a high percentage of Cu<sub>Z</sub> nor N<sub>2</sub>OR containing a high percentage of Cu<sub>Z</sub><sup>\*</sup> shows high enough specific activity in steady-state assays to be consistent with N<sub>2</sub>OR activity in whole cells.<sup>17, 23</sup> N<sub>2</sub>OR containing Cu<sub>Z</sub> can be activated by prolonged dialysis against base,<sup>23</sup> while N<sub>2</sub>OR that contains Cu<sub>Z</sub><sup>\*</sup> can be reductively activated by preincubation with methyl viologen, which reduces Cu<sub>Z</sub><sup>\*</sup> to the active fully reduced (4Cu<sup>I</sup>) redox state.<sup>24, 25</sup> After activation, both Cu<sub>Z</sub> and Cu<sub>Z</sub><sup>\*</sup> show specific activities consistent with whole cell N<sub>2</sub>OR activity.<sup>20, 23</sup> However, it has recently been shown that the Cu<sub>Z</sub><sup>\*</sup> site in its fully reduced redox state is the form of the cluster that is responsible for the rapid N<sub>2</sub>O reduction in steady state assays with methyl viologen, based on its rapid single turnover reaction with N<sub>2</sub>O. Alternatively, in single turnover studies Cu<sub>Z</sub> in its 1-hole redox state reduces N<sub>2</sub>O but at a rate too slow to be catalytically relevant (10<sup>-6</sup> that of the fully reduced state of Cu<sub>Z</sub><sup>\*</sup>).<sup>26</sup> Thus, the physiological role of the Cu<sub>Z</sub> site in nitrous oxide reduction and whether it participates in N<sub>2</sub>O reduction *in vivo* are unknown.

The Cu<sub>Z</sub> site in nitrous oxide reductase has been extensively studied in N<sub>2</sub>OR isolated from *Pseudomonas stutzeri* (PsN<sub>2</sub>OR)<sup>27, 28</sup> and *Paracoccus pantotrophus* (PpN<sub>2</sub>OR).<sup>19, 29</sup> In the latter enzyme, Cu<sub>Z</sub> has been shown to access two redox states, the resting 2Cu<sup>I</sup>2Cu<sup>II</sup> (2-hole) redox state, and a 1 electron reduced 3Cu<sup>I</sup>Cu<sup>II</sup> (1-hole) redox state (E<sup>0</sup> = +60 mV).<sup>19</sup>

Both redox states of Cu<sub>Z</sub> have previously been studied using EPR, absorption, MCD, and resonance Raman spectroscopies.<sup>19, 28, 30–33</sup> However, these studies were performed before the elucidation of the presence of a second sulfur in the Cu<sub>Z</sub> cluster, and so yielded limited direct insight into the cluster and the protonation state of the edge sulfur. Additionally, the previous studies were performed in the presence of background spectroscopic features from ~30% Cu<sub>Z</sub><sup>\*</sup>, which complicates the analysis.<sup>19, 29</sup> These limitations lead to the conclusion that Cu<sub>Z</sub> and Cu<sub>Z</sub><sup>\*</sup> were very similar and perhaps differed only in the second sphere.<sup>28</sup> These results are now extended and correlated to the structural insight that Cu<sub>Z</sub> contains an additional inorganic sulfur edge ligand.<sup>14</sup> An understanding of the protonation state, electronic structure, and potential reactivity of the Cu<sub>Z</sub> site is necessary to gain insight into its reactivity and role *in vivo*.

This study uses EPR, absorption, MCD and resonance Raman spectroscopies coupled with DFT calculations to determine the protonation state of the edge sulfur ligand in the 1-hole and 2-hole redox states of Cu<sub>Z</sub> in *Marinobacter hydrocarbonoclasticus* N<sub>2</sub>OR (*MhN<sub>2</sub>OR*) and to define the electronic structures of these states. This leads to insight into the nature of the reactivity of the 1-hole and 2-hole states of Cu<sub>Z</sub> and the origin of the spectroscopic similarity between 1-hole Cu<sub>Z</sub> and 1-hole Cu<sub>Z</sub><sup>\*</sup>, despite significant differences in edge ligation in the two sites.

## 2. Methodology

### 2.1 Summary of Experimental Methodology

Full experimental methodology and computational details can be found in the Electronic Supporting Information, while a summary is presented here. Nitrous oxide reductase (N<sub>2</sub>OR) was isolated from *Marinobacter hydrocarbonoclasticus* 617 (formerly *Pseudomonas nautica*) grown under microaerobic conditions in the presence of nitrate after two aerobic chromatographic steps without added reductant, as described previously.<sup>17</sup> These purification conditions were shown to maximize the amount of Cu<sub>4</sub>S<sub>2</sub> Cu<sub>Z</sub> content relative to Cu<sub>4</sub>S Cu<sub>Z</sub><sup>\*</sup> in the purified enzyme. Samples containing larger amounts of Cu<sub>Z</sub><sup>\*</sup> were purified in parallel with three chromatographic purification steps from a batch of cells grown under anaerobic conditions in the presence of nitrate, and that had been stored at –80 °C for a long period.<sup>17, 26</sup> Both *MhN<sub>2</sub>OR* showed copper quantitation results consistent with fully occupancy of the Cu<sub>A</sub> and Cu<sub>Z</sub>/Cu<sub>Z</sub><sup>\*</sup> sites (6.4±0.2 and 6.2±0.7 respectively). The percentage of Cu<sub>Z</sub> versus Cu<sub>Z</sub><sup>\*</sup> in the samples used for this study was determined by EPR spin quantitation (Figure S1). Samples purified with high amounts of Cu<sub>Z</sub> contained 60±10% Cu<sub>Z</sub>, while samples purified to obtain more Cu<sub>Z</sub><sup>\*</sup> contained 10±10% Cu<sub>Z</sub>. Spectroscopic samples of 1-hole and 2-hole Cu<sub>Z</sub> were prepared in a glove box under N<sub>2</sub> atmosphere. Samples of 1-hole Cu<sub>Z</sub> were prepared from *MhN<sub>2</sub>OR* (60% Cu<sub>Z</sub> and 40% Cu<sub>Z</sub><sup>\*</sup>) that had been incubated with 100 equivalents of reduced methyl viologen, with subsequent removal of the methyl viologen using a desalting column. Samples of 2-hole Cu<sub>Z</sub> were prepared by reducing *MhN<sub>2</sub>OR* (60±10% Cu<sub>Z</sub>, 40±10% Cu<sub>Z</sub><sup>\*</sup>) with 10 equivalents of sodium ascorbate, which reduces the Cu<sub>A</sub> site rapidly and the 2-hole Cu<sub>Z</sub> site very slowly, and spectra were collected within 1 hour so that minimal reduction of 2-hole Cu<sub>Z</sub> was observed. In parallel, *MhN<sub>2</sub>OR* samples containing 90±10% Cu<sub>Z</sub><sup>\*</sup> were reduced

with 10 equivalents of sodium ascorbate to obtain the spectral features of 1-hole  $\text{Cu}_Z^*$ . For pH and deuteration studies, samples of 1-hole and 2-hole  $\text{Cu}_Z$  were buffer exchanged by centrifugation into different pH or pD buffers. Typical  $MhN_2OR$  concentrations used for spectroscopic samples were 0.1–0.3 mM for absorption, MCD and EPR, and up to 0.5 mM for resonance Raman.

## 2.2 Computational Modeling

A computational model of  $\text{Cu}_Z$  was built from the atomic coordinates of the crystal structure of *Pseudomonas stutzeri*  $N_2OR$ , the only known structure of the  $\text{Cu}_4\text{S}_2$  cluster (PDB ID 3SBP, resolution 1.7 Å).<sup>14</sup> The model included the  $\text{Cu}_4\text{S}_2$  core and 7 ligating His residues, where the  $\alpha$  carbon and distal nitrogen were constrained at their crystallographic positions. A computational model for  $\text{Cu}_Z^*$  with a hydroxide bridging ligand and identical  $\alpha$  carbon and distal nitrogen constraints was constructed from the crystal structure of *Paracoccus denitrificans*  $N_2OR$  (*PdN\_2OR*, PDB ID 1FWX).<sup>13</sup> Calculations were performed using Gaussian 09 (version d01).<sup>34</sup> Geometry optimizations were performed using the B3LYP functional, the TZVP basis set on all core atoms ( $\text{Cu}_4\text{S}$ ) and the ligating His nitrogens, and the SV basis set on all remaining atoms, and solvation was modeled with a PCM of 4.0. A larger basis set and different functionals were also explored, as described in the text. The optimized structures were then used for frequency, TD DFT, and single point calculations. To determine the relative energy of deprotonation ( $\Delta E$ ) of the edge  $\text{SH}^-$  in the 2-hole versus 1-hole redox state, larger models were optimized that included two second sphere carboxylates, Asp127 and Asp240, which hydrogen bond to the His ligands of  $\text{Cu}_I$  and  $\text{Cu}_{II}$ . The energy of an internal proton transfer from the edge  $\text{SH}^-$  to Asp127 was calculated for the 1-hole and 2-hole redox states and compared to obtain the  $\Delta E$ .

## 3 Results and Analysis

### 3.1 Spectroscopy of 1-hole $\text{Cu}_Z$

Previous spectroscopic studies of  $\text{Cu}_Z$ , undertaken before identification of the presence of a second sulfur, were performed on samples of *PpN\_2OR* and *PsN\_2OR* that contained mixtures of the  $\text{Cu}_Z$  and  $\text{Cu}_Z^*$  sites (in a 7:3 ratio for *PpN\_2OR*) without a way to resolve the spectral features of the  $\text{Cu}_Z$  site from the mixture.<sup>19, 28, 29</sup> Recently, it has been found that the two-sulfur  $\text{Cu}_Z$  site cannot be reduced by methyl viologen, which reduces both the  $\text{Cu}_A$  site and the  $\text{Cu}_Z^*$  form of the cluster.<sup>26</sup> This provides an opportunity to cleanly resolve the spectral features of 1-hole  $\text{Cu}_Z$  by studying methyl viologen reduced samples after removal of the reductant. This approach allows correlation of the electronic structure of 1-hole  $\text{Cu}_Z$ , obtained from spectroscopy, with the recently determined  $\text{Cu}_4\text{S}_2$  structure of the cluster, to determine the nature of the edge sulfur ligand in its 1-hole and resting 2-hole redox states. **EPR** The X-band and Q-band EPR spectra of a methyl viologen reduced sample of 1-hole  $\text{Cu}_Z$  are given in Figure 2. The EPR spectrum is axial with  $g_{\parallel} > g_{\perp} > 2.0$  and a pattern of five evenly spaced hyperfine lines in the  $A_{\parallel}$  region. The axial nature of the spectrum indicates that, while the spin density is delocalized over multiple copper nuclei, it resides in dominantly  $d_{x^2-y^2}$  orbitals on each Cu site that contributes to the ground state. The  $A_{\parallel}$  hyperfine features can be further resolved in the second derivative of the X-band EPR spectrum, as can hyperfine features in the  $A_{\perp}$  region (Figure 2A inset and Figure S2).

Simulation of the X-band, X-band 2nd derivative, and Q-band EPR spectra yields the  $g$  and  $A$  values for 1-hole  $\text{Cu}_Z$  given in Table 1. The  $g$  values for 1-hole  $\text{Cu}_Z$  are very similar to those previously obtained for 1-hole  $\text{Cu}_Z^*$  (Table 1) and to those obtained for  $\text{Cu}_Z$  in  $PpN_2OR$ .<sup>15, 29</sup> This is interesting, considering that an edge  $\text{SH}^-$  (thiolate) or  $\text{S}^{2-}$  (sulfide) in  $\text{Cu}_Z$  would be expected to be a more covalent ligand than the hydroxide in  $\text{Cu}_Z^*$ <sup>15</sup> and this would lower the  $g$  values. However, in 1-hole  $\text{Cu}_Z^*$  there is a high energy d-d transition that is not present in the 1-hole  $\text{Cu}_Z$  spectrum (vide infra). This transition has previously been assigned as a  $d_{xy} \rightarrow d_{x^2-y^2}$  excitation localized on  $\text{Cu}_I$ .<sup>35</sup> The  $g_{\parallel}$  value is inversely proportional to the  $d_{xy}$  to  $d_{x^2-y^2}$  energy splitting, so the presence of a high energy  $d_{xy} \rightarrow d_{x^2-y^2}$  transition in  $\text{Cu}_Z^*$  but not in  $\text{Cu}_Z$  would lead to a lower  $g_{\parallel}$  value for  $\text{Cu}_Z^*$  than would be expected from covalency alone, which could result in similar  $g_{\parallel}$  values between 1-hole  $\text{Cu}_Z^*$  and the more covalent 1-hole  $\text{Cu}_Z$  site. The ligand field origin of the lower energy  $d_{xy} \rightarrow d_{x^2-y^2}$  transition in 1-hole  $\text{Cu}_Z$  is considered below.

The  $A_{\parallel}$  and  $A_{\perp}$  values for 1-hole  $\text{Cu}_Z$  are similar in magnitude to those for  $\text{Cu}_Z^*$ , but fitting the hyperfine pattern requires three equivalent contributions rather than the ~5:2 ratio of hyperfine values observed for  $\text{Cu}_Z^*$  (Table 1).<sup>36</sup> This indicates that in the ground state of 1-hole  $\text{Cu}_Z$  the spin is distributed over three copper centers in dominantly  $d_{x^2-y^2}$  orbitals. The three coppers involved are likely  $\text{Cu}_I$ ,  $\text{Cu}_{II}$ , and  $\text{Cu}_{IV}$ , since these copper centers are in the same plane as the two sulfur ligands and bonding with the strong donor  $\mu_4$  sulfide and  $\mu_2$  sulfur ligands should define a common  $x, y$  plane for these coppers, with the  $z$  axis of the local  $g$  tensor of each copper oriented perpendicular to the  $\text{Cu}_3\text{S}_2$  plane. This is consistent with the axial nature of the  $g$  values and with the DFT calculations reported below.

**Absorption and MCD**—The low temperature absorption and MCD spectra of a methyl viologen reduced sample of 1-hole  $\text{Cu}_Z$  are presented in Figure 3A. The absorption maximum of 1-hole  $\text{Cu}_Z$  occurs at  $14,600 \text{ cm}^{-1}$  ( $\epsilon \approx 3,000 \text{ M}^{-1} \text{ cm}^{-1}$ ),  $1,000 \text{ cm}^{-1}$  lower than the absorption maximum of 1-hole  $\text{Cu}_Z^*$  (Figure 3B). There are no additional low energy intense absorption features due to the edge sulfur. The low temperature absorption and MCD spectra can be simultaneously fit to yield a total of 11 transitions, which can be assigned by considering their energies and  $C_0/D_0$  ratios, following Ref. <sup>15</sup> (Table S1). Comparison of the transition assignments and energies of the 1-hole  $\text{Cu}_Z$  and 1-hole  $\text{Cu}_Z^*$  sites reveals some key differences. While the absorption maximum of  $\text{Cu}_Z$  occurs at lower energy than that of  $\text{Cu}_Z^*$ , from MCD the three  $\mu_4\text{S}$  to Cu CT transitions, assigned in  $\text{Cu}_Z^*$ ,<sup>35</sup> occur at very similar energies in the two sites (bands 5, 6, and 7, numbering given in Figure 3). The shift in the absorption maximum therefore arises from a different intensity pattern for these transitions, where in  $\text{Cu}_Z$  the lowest energy transition at  $14,600 \text{ cm}^{-1}$  is the most intense (band 5) and the transition at  $15,600 \text{ cm}^{-1}$  is weaker (band 6), but in  $\text{Cu}_Z^*$  this is reversed. The  $\mu_4\text{S}^{2-}$  to Cu CTs in  $\text{Cu}_Z^*$  have previously been assigned as transitions from the three different 3p orbitals of the  $\mu_4\text{S}^{2-}$  to the  $\beta$  LUMO of the cluster. From our current study of resting 1-hole  $\text{Cu}_Z^*$  and  $\text{Cu}_Z$  with different edge ligands,<sup>15, 35</sup> the  $\beta$  LUMO is delocalized in the plane that contains  $\text{Cu}_I$ ,  $\text{Cu}_{II}$ ,  $\text{Cu}_{IV}$  and the  $\mu_4\text{S}^{2-}$ , with different amounts of spin distributed over  $\text{Cu}_I$ ,  $\text{Cu}_{II}$ , and  $\text{Cu}_{IV}$  depending on the edge ligation. Two of the  $\mu_4\text{S}^{2-}$  p orbitals are in the plane, oriented between  $\text{Cu}_I$  and  $\text{Cu}_{IV}$  ( $\text{S } p_x$ ) and between  $\text{Cu}_{IV}$  and  $\text{Cu}_{II}$  ( $\text{S } p_y$ ), while the third is perpendicular to the plane ( $\text{S } p_z$ ). Scheme S1 reflects the

orientation and simplified composition of these orbitals determined for 1-hole  $\text{Cu}_Z^*$  from DFT calculations. The CT intensities reflect the overlap of these three S p orbitals with the  $\beta$  LUMO. Since bands 5 and 6 show the highest intensity in the 1-hole forms of  $\text{Cu}_Z$  and  $\text{Cu}_Z^*$ , these must reflect charge transfer from the in-plane S  $p_{x'}$  (band 6, dominant in  $\text{Cu}_Z^*$  due to higher overlap with  $\text{Cu}_I$ ) and S  $p_{y'}$  (band 5) orbitals. Bands 6 and 5 form a pseudo-A feature in the MCD spectrum (i.e. derivative-shaped) and thus must arise from two transitions with orthogonal transition moments that spin-orbit couple in a third, mutually perpendicular direction (i.e.  $L_z$ ). Since band 6 arises from a transition to  $\text{Cu}_I$  (from its dominant intensity in  $\text{Cu}_Z^*$ ), band 5 must reflect a transition to  $\text{Cu}_{IV}$ , since the  $\text{Cu}_I$ -S and  $\text{Cu}_{IV}$ -S bonds are close to perpendicular ( $96^\circ$  from crystallography) while the  $\text{Cu}_I$ -S and  $\text{Cu}_{II}$ -S bonds are close to parallel ( $160^\circ$ ).<sup>13</sup> The change in relative intensities of the  $\mu_4\text{S}^{2-}$  to Cu CT transitions in  $\text{Cu}_Z$  relative to  $\text{Cu}_Z^*$ , where band 6 decreases in intensity while band 5 increases in intensity, thus indicates that there is less spin on  $\text{Cu}_I$  and more spin on  $\text{Cu}_{IV}$  in 1-hole  $\text{Cu}_Z$  relative to 1-hole  $\text{Cu}_Z^*$ . This is consistent with the EPR hyperfine values, which suggest that the spin in  $\text{Cu}_Z$  is delocalized 1:1:1 over  $\text{Cu}_I$ ,  $\text{Cu}_{II}$ , and  $\text{Cu}_{IV}$ , while from Ref. <sup>35</sup> in  $\text{Cu}_Z^*$  the spin is delocalized  $\sim 5:2$  over  $\text{Cu}_I$  and  $\text{Cu}_{IV}$ . Additionally, in  $\text{Cu}_Z^*$ , a band at  $18,000\text{ cm}^{-1}$  (band 8) was assigned as a high energy d-d transition due to its high  $C_0/D_0$  ratio; this was assigned as a localized  $d_{xy} \rightarrow d_{x^2-y^2}$  transition on  $\text{Cu}_I$ , where most of the 1-hole is localized.<sup>35</sup> No equivalent high energy d-d transition is observed in the MCD spectrum of  $\text{Cu}_Z$ . The lower energy of the d-d transitions in  $\text{Cu}_Z$  relative to  $\text{Cu}_Z^*$  is likely due to the decreased spin on  $\text{Cu}_I$ , the only four coordinate site, relative to  $\text{Cu}_{II}$  and  $\text{Cu}_{IV}$ , which are both 3 coordinate and have a weaker ligand field.

**Resonance Raman**—The resonance Raman spectrum of 1-hole  $\text{Cu}_Z$  and the enhancement profiles of the vibrations are presented in Figures 4A and 4B, respectively. Seven vibrations are enhanced in the most intense S to Cu CT transition (band 5), including three intense vibrations at  $203$ ,  $378$ , and  $492\text{ cm}^{-1}$ . The vibration at  $378\text{ cm}^{-1}$  occurs at the same energy as a Cu-S stretch of the  $\text{Cu}_Z^*$  site (Figure S3) and the previously reported <sup>34</sup>S isotope sensitivities of both vibrations are similar ( $-5.8$  and  $-4.7\text{ cm}^{-1}$ , respectively),<sup>28</sup> indicating that the  $378\text{ cm}^{-1}$  vibration in 1-hole  $\text{Cu}_Z$  can be assigned as a Cu-S vibration of the  $\mu_4$  sulfide. In contrast, the  $203\text{ cm}^{-1}$  vibration is significantly lower in energy than the vibrations of  $\text{Cu}_Z^*$ , and thus can be assigned as a Cu-S vibration of the  $\mu_2$  sulfur ligand that is only present in  $\text{Cu}_Z$ . Further, there are two high energy vibrations in  $\text{Cu}_Z$  at  $450$  and  $492\text{ cm}^{-1}$  that show significant deuterium isotope sensitivity, shifting down in energy by  $-137\text{ cm}^{-1}$  (for the  $492\text{ cm}^{-1}$  vibration) in deuterated buffer (Figure 4C). This shift requires their assignment as S-H bending modes. Thus, we can definitively identify the edge ligand in 1-hole  $\text{Cu}_Z$  as a  $\mu_2\text{SH}^-$ . The S-H bending modes at  $492$  and  $450\text{ cm}^{-1}$  are present at both pH 7.8 and pH 10 (Figure 4D), indicating that the pKa of the edge thiolate is  $\sim 11$  or higher. This is further supported by the lack of pH dependence observed in the MCD and EPR spectra of 1-hole  $\text{Cu}_Z$  between pD 6 and pD 10 (Figure S4). Since the second pKa of free hydrogen sulfide in water is 12, a pKa range of 11–12 can be estimated for the edge thiolate ligand in 1-hole  $\text{Cu}_Z$ .

### 3.2 Spectroscopy of 2-hole Cu<sub>Z</sub>

**Absorption**—The 2-hole redox state has been previously shown to be the resting redox state of Cu<sub>Z</sub>. 2-hole Cu<sub>Z</sub> is diamagnetic from MCD.<sup>19</sup> The absorption features of 2-hole Cu<sub>Z</sub> in as-isolated N<sub>2</sub>OR are present with additional spectral contributions from oxidized Cu<sub>A</sub> and some amount of 1-hole Cu<sub>Z</sub>\*.<sup>26</sup> To remove these contributions, the absorption spectrum of 2-hole Cu<sub>Z</sub> (Figure 5) was obtained after reduction with sodium ascorbate, which reduces the Cu<sub>A</sub> site faster than it reduces 2-hole Cu<sub>Z</sub>, and subtraction of the spectral contribution of 1-hole Cu<sub>Z</sub>\*, obtained from a separately purified N<sub>2</sub>OR sample containing 90±10% Cu<sub>Z</sub>\*. An intense absorption maximum for 2-hole Cu<sub>Z</sub> is observed at 18,300 cm<sup>-1</sup> ( $\epsilon \approx 10,000$  M<sup>-1</sup> cm<sup>-1</sup>) with a weaker low energy shoulder, consistent with absorption spectra previously reported for ascorbate reduced samples containing high amounts of 2-hole Cu<sub>Z</sub>.<sup>19, 32</sup> The low temperature absorption spectrum of 2-hole Cu<sub>Z</sub> (Figure S5) resolves this absorption maximum into three distinct absorption bands. Simulation of the room temperature absorption spectrum with transition energies derived from the low temperature spectrum distinguishes five transitions, all with absorption intensities higher than 1,000 M<sup>-1</sup> cm<sup>-1</sup>, sufficiently intense to be S to Cu CT transitions from the  $\mu_4S^{2-}$  or the  $\mu_2S$  ligand (Figure 5). The two most intense transitions (bands 2 and 3) are either from different ligands ( $\mu_2S$  and  $\mu_4S^{2-}$ ) or from the same ligand to two different acceptor orbitals (the  $\alpha$  and  $\beta$  holes of the broken symmetry singlet ground state). Based on the correlation of resonance Raman excitation profiles of the vibrations of 2-hole Cu<sub>Z</sub> to DFT calculations (vide infra), the assignment of the two transitions as CT transitions from the  $\mu_4S^{2-}$  to two different holes is preferred.

**Resonance Raman**—The resonance Raman spectrum of 2-hole Cu<sub>Z</sub> was obtained upon excitation into the intense absorption maximum at 18,300 cm<sup>-1</sup> (Figure 6A). Two vibrations are enhanced at 350 and 405 cm<sup>-1</sup>. The <sup>34</sup>S isotope shifts of these vibrations have been previously reported to be -5.6 and -5.8 cm<sup>-1</sup>, respectively, indicating that they are Cu-S stretches.<sup>28</sup> In contrast to 1-hole Cu<sub>Z</sub>, no higher energy S-H bending vibration is observed (up to 800 cm<sup>-1</sup>). The excitation profile of the Cu-S stretching vibrations shows that they are enhanced differently in the most intense absorption bands 2 and 3 (Figure 6B). The lower energy vibration at 350 cm<sup>-1</sup> is enhanced in both transitions, while the higher energy vibration at 405 cm<sup>-1</sup> is dominantly enhanced in the lower energy transition (band 2) and only weakly enhanced in band 3. This difference in profiling behavior is consistent with the Cu-S vibrations obtained computationally for a Cu<sub>4</sub>S<sub>2</sub> cluster with a  $\mu_2S^{2-}$  and  $\mu_4S^{2-}$  and with the predicted enhancements of key vibrations in transitions from the  $\mu_4S^{2-}$  to the  $\alpha$  and  $\beta$  holes (see 3.3).

The resonance Raman spectrum 2-hole Cu<sub>Z</sub> shows no significant shift in the energies of the 350 and 405 cm<sup>-1</sup> vibrations between pD 6 and pD 10 (Figure S6). This suggests that the edge ligand has a pKa either lower than 5.5 or higher than 10.5. A pKa higher than 10.5 in the 2-hole redox state is not consistent with observed pKa of 11–12 for 1-hole Cu<sub>Z</sub>, as the increased charge of the 2-hole state will lead to a lower pKa relative to the 1-hole redox state. The possibility of a pKa less than 5.5 for 2-hole Cu<sub>Z</sub> is evaluated computationally below.

### 3.3 Calculations

**1-hole Cu<sub>Z</sub>**—A computational model of 1-hole Cu<sub>Z</sub> was constructed based on the crystal structure of *Pseudomonas stutzeri* N<sub>2</sub>OR (PDB ID 3SBP, resolution 1.7 Å).<sup>14</sup> On the basis of the resonance Raman data, the edge sulfur was modeled as an SH<sup>-</sup> ligand bridging the Cu<sub>I</sub>-Cu<sub>IV</sub> edge (Figure 7A). This will be compared to an experimentally validated model of the Cu<sub>Z</sub>\* site, which has a hydroxide ligand bridging the Cu<sub>I</sub>-Cu<sub>IV</sub> edge (Figure 7B).<sup>15</sup> The optimized structure of the 1-hole SH<sup>-</sup> cluster agrees well with the bond lengths and angles observed in the crystal structure (2.35 Å and 2.48 Å for the Cu<sub>I</sub>-μ<sub>2</sub>SH<sup>-</sup> and Cu<sub>IV</sub>-μ<sub>2</sub>SH<sup>-</sup> bonds computationally, relative to 2.61 Å and 2.49 Å crystallographically with a resolution of 1.7 Å,<sup>14</sup> Table S2). Since the crystal was grown from the “purple” resting form of *Ps*N<sub>2</sub>OR, containing the resting 2-hole redox state of the Cu<sub>Z</sub> site, the Cu<sub>Z</sub> site in the crystal may have some photo-reduction due to exposure to X-ray radiation.<sup>37</sup> The calculated structures and spin distributions are not significantly perturbed when a triple zeta basis set was used on all His ring atoms (Tables S4 and S5). Including the second sphere residues Lys397 and Glu435 in the computational model also does not affect the structure or spin distribution, consistent with the small effect on the spectral features of 1-hole Cu<sub>Z</sub>\* observed experimentally upon deprotonation of Lys397.<sup>15</sup> Thus, the structures including only first sphere ligands were used to model the Cu<sub>Z</sub> and Cu<sub>Z</sub>\* sites in this study.

The 1-hole model with an SH<sup>-</sup> edge ligand reproduces the key spectral features observed for the 1-hole Cu<sub>Z</sub> site. The Mulliken atomic spin distribution of the cluster with an SH<sup>-</sup> edge ligand is delocalized over Cu<sub>I</sub>, Cu<sub>II</sub>, and Cu<sub>IV</sub> in a 2:1:1 ratio. In going from Cu<sub>Z</sub>\* to Cu<sub>Z</sub> the calculated spin on Cu<sub>I</sub> changes from 26% to 17% (Table 2), which is consistent with the decrease in intensity of band 6 observed in the absorption and MCD data for 1-hole Cu<sub>Z</sub> and leads to a more equal distribution of spin over Cu<sub>I</sub>, Cu<sub>II</sub>, and Cu<sub>IV</sub>, consistent with the EPR hyperfine values. The LUMO of the Cu<sub>Z</sub> model contains d<sub>x<sup>2</sup>-y<sup>2</sup></sub> character on Cu<sub>I</sub>, Cu<sub>II</sub>, and Cu<sub>IV</sub>, which are aligned, consistent with the ground state predicted from the EPR g values (Figure S7). It also contains significant antibonding μ<sub>4</sub>S<sup>2-</sup> and μ<sub>2</sub>SH<sup>-</sup> character, explaining why Cu-S stretching vibrations of both the μ<sub>4</sub>S<sup>2-</sup> and μ<sub>2</sub>SH<sup>-</sup> are enhanced in the charge transfer transitions to this acceptor orbital. Additionally, the computational model predicts the Cu<sub>Z</sub> site to be more covalent than the Cu<sub>Z</sub>\* site, with 10% less Cu character in the ground state wavefunction, reflecting delocalization of the spin from Cu<sub>I</sub> onto the edge SH<sup>-</sup> ligand. The low g<sub>||</sub> value for 1-hole Cu<sub>Z</sub> is also predicted by the computational model (Table S7). However, in contrast to experiment, the calculated g<sub>||</sub> values for the Cu<sub>Z</sub> and Cu<sub>Z</sub>\* models differ, with a higher calculated g<sub>||</sub> value for Cu<sub>Z</sub>\* than that observed experimentally. This suggests that the calculated model of Cu<sub>Z</sub>\* does not accurately predict the ligand field on Cu<sub>I</sub> that leads to the higher energy d<sub>xy</sub> → d<sub>x<sup>2</sup>-y<sup>2</sup></sub> transition observed experimentally.

The Cu-S stretching vibrations and S-H bending vibrations for the 1-hole SH<sup>-</sup> model of Cu<sub>Z</sub> are given in Table S8 and Figure S8. The model predicts two S-H bending modes at 426 and 461 cm<sup>-1</sup> with H/D isotope shifts of -125 cm<sup>-1</sup> and -123 cm<sup>-1</sup>, respectively, similar to the vibrations observed experimentally at 450 and 492 cm<sup>-1</sup> (with a shift of -135 cm<sup>-1</sup> for the 492 cm<sup>-1</sup> vibration; the 450 cm<sup>-1</sup> vibration cannot be observed after deuteration due to overlap with the ice scattering peak). Equivalent O-H bends are predicted for the OH bridged Cu<sub>Z</sub>\* model at higher energies, but these are not experimentally observed. The Cu<sub>Z</sub>



model also predicts the presence of a low energy Cu-S stretching vibration of the  $\mu_2\text{SH}^-$  ( $178\text{ cm}^{-1}$ , observed at  $203\text{ cm}^{-1}$  experimentally) and both models show similar energies for the Cu- $\mu_4\text{S}$  stretching vibrations. The absolute energies of the Cu-S stretching vibrations for both the  $\mu_4$  sulfide and  $\mu_2$  thiolate are underestimated, as has been found for computational models of the  $\text{Cu}_Z^*$  site.<sup>15, 35</sup> The TD DFT calculated absorption spectrum for the  $\text{Cu}_Z$  model is also very similar to the calculated absorption spectrum for the  $\text{Cu}_Z^*$  model both with B3LYP and with the functional B98, which has been shown to predict the experimental absorption spectrum of a  $\text{Cu}_3\text{S}_2$  model complex reasonably well.<sup>38</sup> Interestingly, neither the experimental absorption spectrum nor the TD-DFT calculation predicts an intense low energy charge transfer transition from the  $\mu_2\text{SH}^-$  ligand (Figure S9). While some weak transitions predicted computationally at lower energy than the  $\mu_4\text{S}^{2-}$  to Cu CT transitions have  $\mu_2\text{SH}^-$  to Cu CT character, they are predicted to lack intensity and are thus difficult to distinguish from the Cu d to d transitions that are also observed in this energy region.

Thus, a computational model of the tetranuclear copper cluster with an  $\text{SH}^-$  edge ligand bridging  $\text{Cu}_I$  and  $\text{Cu}_{IV}$  provides a good structural model of 1-hole  $\text{Cu}_Z$  that reproduces its key spectral features. This spectroscopically calibrated model was then extended to the 2-hole redox state of the  $\text{Cu}_Z$  site, for which less experimental data are accessible.

**2-hole  $\text{Cu}_Z$** —Two possible computational models were developed for 2-hole  $\text{Cu}_Z$ , one with an edge thiolate ligand ( $\text{Cu}_4\text{S}(\text{SH})$ ) and one with an edge sulfide ( $\text{Cu}_4\text{S}_2$ ). These were optimized in both the triplet ( $S=1$ ) and broken symmetry singlet ( $S=0$ ) ground spin states. For both models the singlet is lower in electronic energy, by  $-8.0\text{ kcal/mol}$  for the sulfide and  $-3.4\text{ kcal/mol}$  for the thiolate (spin corrected energies using B3LYP). The singlet state was verified to be the ground state using a variety of functionals, including M06L, M06, and TPSSh. Thus, both structures would be consistent with the experimentally determined singlet ground state of 2-hole  $\text{Cu}_Z$ .<sup>19</sup> The optimized structure of the 2-hole  $\text{Cu}_4\text{S}(\text{SH})$  model is similar to that of the 1-hole  $\text{SH}^-$  model of 1-hole  $\text{Cu}_Z$ , with slightly shorter  $\text{Cu}_I/\text{Cu}_{IV}\text{-SH}^-$  and  $\text{Cu}_I/\text{Cu}_{IV}\text{-}\mu_4\text{S}$  bonds (Table S9). The  $\alpha$  LUMO is dominantly localized on  $\text{Cu}_I$  and has equal  $\mu_4\text{S}^{2-}$  and  $\mu_2\text{SH}^-$  antibonding character (Table 3) while the  $\beta$  LUMO is delocalized equally over  $\text{Cu}_{II}$  and  $\text{Cu}_{IV}$  and has more  $\mu_4\text{S}^{2-}$  antibonding character. Upon deprotonation of the edge  $\text{SH}^-$ , the 2-hole  $\text{Cu}_4\text{S}_2$  model has significantly shorter bonds between the edge sulfide and  $\text{Cu}_I/\text{Cu}_{IV}$  and similar  $\mu_4\text{S}^{2-}\text{-Cu}$  bond lengths to the 2-hole  $\text{SH}^-$  model (Table S9). In this model, the  $\alpha$  LUMO is localized on  $\text{Cu}_I$  while the  $\beta$  LUMO is localized on  $\text{Cu}_{IV}$  (Figure 8 and Table 3). Both holes have significant  $\mu_2\text{S}^{2-}$  character, indicating that the edge sulfide copper bonds are highly covalent.

The energy of deprotonation calculated from the 2-hole models was compared to the calculated energy of deprotonation of the 1-hole  $\text{SH}^-$  model, where the experimentally estimated pKa of the edge thiolate is 11–12 (vide supra). Examination of the energy required to deprotonate the 1-hole and 2-hole  $\text{SH}^-$  models shows that deprotonation of the 1-hole is not energetically favored ( $\Delta E = 26\text{ kcal/mol}$ , relative to an energy of  $-268\text{ kcal/mol}$  for a solvated proton)<sup>39</sup> while deprotonation of the 2-hole is favorable ( $\Delta E = -9\text{ kcal/mol}$ ). However, the two models have different charges ( $+2/+1$  and  $+3/+2$  for protonated and deprotonated 1-hole and 2-hole models, respectively) and this will significantly affect the relative energies of deprotonation. To minimize the charge effect, the computational models

were expanded to include two second sphere Asp residues near the  $\text{Cu}_Z$  site, such that the 1-hole  $\text{Cu}_Z$  model with an edge thiolate is neutral and the 2-hole  $\text{Cu}_Z \text{Cu}_4\text{S}(\text{SH})$  model has a +1 charge. The proton transfer was performed internally to one of the Asp residues, so the total charge of the model does not change upon deprotonation (Figure S10). The  $\Delta E$  for deprotonation of the 2-hole edge thiolate relative to the 1-hole species is calculated to be  $-25$  kcal/mol (with a dielectric of 4.0). This value is dependent on the dielectric (Figure S11) and, at high dielectric values, converges to a  $\Delta E$  of  $-12$  kcal/mol. To estimate the difference in pKa between 1-hole and 2-hole  $\text{Cu}_Z$ , the  $\Delta G$  was estimated from the  $\Delta E$  using frequency calculations for structures with identical fixed atom constraints and thus the same number and magnitude of imaginary frequencies (these  $\Delta G$  corrections vary by only 0.3 kcal/mol between the protonated and deprotonated 1-hole structures). This gives a  $\Delta G$  of  $-12$  kcal/mol for deprotonation of 2-hole versus 1-hole  $\text{Cu}_Z$ , which corresponds to a pKa of  $-9$ . Given the experimental pKa value of 11–12 for the edge thiolate in 1-hole  $\text{Cu}_Z$ , these calculations predict a pKa for a thiolate in 2-hole  $\text{Cu}_Z$  of 3 or less, consistent with the absence of a pH effect in resonance Raman of 2-hole  $\text{Cu}_Z$  at pD 6. This strongly suggests that 2-hole  $\text{Cu}_Z$  is a two sulfide cluster at neutral pH.

The calculated spectral features for the  $\text{Cu}_4\text{S}_2$  2-hole  $\text{Cu}_Z$  model can be compared with those determined experimentally. The TD DFT predicted absorption spectrum (using both B3LYP and B98) is qualitatively similar to the experimental absorption spectrum, showing two intense absorption maxima with a higher energy shoulder (Figure S12). The predicted vibrations of the 2-hole  $\text{Cu}_4\text{S}_2$  model are given in Table S10 and Figure S13. All of the calculated vibrations are shifted up in energy in comparison to those of the 1-hole  $\text{SH}^-$  model, with the most significant energy differences observed for the sulfur edge vibrations, due to the short and highly covalent  $\text{Cu}-\mu_2\text{S}^{2-}$  bonds in the 2-hole  $\text{Cu}_4\text{S}_2$  cluster. In particular, the  $\mu_2\text{S}^{2-}-\text{Cu}_I$  stretch now occurs at a similar energy to and mixes with vibrations of the  $\mu_4\text{S}^{2-}$ , leading to symmetric and antisymmetric combinations of the  $\mu_2\text{S}^{2-}-\text{Cu}_I$  and  $\mu_4\text{S}^{2-}-\text{Cu}_I$  stretches (predicted at 312 and 309  $\text{cm}^{-1}$ , respectively, see SI). The symmetric combination is allowed in resonance Raman and will be enhanced in all transitions due to the high amount of  $\mu_2\text{S}^{2-}$  character in both the  $\alpha$  and  $\beta$  holes. This is a good candidate for the 350  $\text{cm}^{-1}$  vibration observed experimentally that profiles in both intense absorption bands (see Figure 6B). The highest energy core vibration of the 2-hole  $\mu_2\text{S}^{2-}$  cluster is a symmetric  $\text{Cu}_{II}-\mu_4\text{S}^{2-}-\text{Cu}_{IV}$  stretch predicted at 344  $\text{cm}^{-1}$  which will be selectively enhanced in a transition to the  $\beta$  LUMO localized on  $\text{Cu}_{IV}$  (Figure 8). A symmetric  $\text{Cu}_{II}-\mu_4\text{S}^{2-}-\text{Cu}_{IV}$  stretch is also computationally predicted in the 1-hole  $\text{SH}^-$  model at 320  $\text{cm}^{-1}$  and the calculated shift in energy of this mode between the 1-hole and 2-hole models (+24  $\text{cm}^{-1}$ ) is similar to the energy increase of the highest energy Cu-S stretches observed experimentally in 1-hole and 2-hole  $\text{Cu}_Z$  (378 and 405  $\text{cm}^{-1}$  respectively,  $\nu$  of +27  $\text{cm}^{-1}$ ). Thus, the 2-hole  $\text{Cu}_4\text{S}_2$  model qualitatively predicts a high energy Cu-S vibration that will be selectively enhanced only in a transition to the  $\beta$  hole and a lower energy Cu-S vibration that will be enhanced in both intense transitions. This is consistent with the enhancement profiles of the two vibrations observed experimentally in Figure 6B. This establishes that a  $\mu_2\text{S}^{2-}$  bridge is energetically favored and consistent with the spectral features of 2-hole  $\text{Cu}_Z$ .

## 4. Discussion

A combination of spectroscopic methods and DFT calculations has been used to define the protonation state of the  $\mu_2$  sulfur ligand on the  $\text{Cu}_I\text{-Cu}_{IV}$  edge in 1-hole and 2-hole  $\text{Cu}_Z$ . This leads to insight into the spectroscopic similarities between 1-hole  $\text{Cu}_Z$  and 1-hole  $\text{Cu}_Z^*$ , the redox reactivity of 1-hole  $\text{Cu}_Z$  in the slow 2 electron reduction of  $\text{N}_2\text{O}$ , and the interconversion between  $\text{Cu}_Z$  and  $\text{Cu}_Z^*$ , the reactive form of the cluster for  $\text{N}_2\text{O}$  reduction *in vitro*.

### 4.1 Protonation states of 1-hole and 2-hole $\text{Cu}_Z$

The protonation state of the edge ligand in 1-hole  $\text{Cu}_Z$  has been directly determined by resonance Raman spectroscopy. Two high energy vibrations are enhanced in the most intense  $\mu_4\text{S}^{2-}$  to Cu CT transition of 1-hole  $\text{Cu}_Z$ , at 450 and 492  $\text{cm}^{-1}$ , and have large isotope shifts upon solvent deuteration ( $-137 \text{ cm}^{-1}$  for the 492  $\text{cm}^{-1}$  mode). This is consistent with S-H bending modes, indicating that the  $\mu_2\text{S}$  ligand is a thiolate. The energy and solvent isotope shift of these S-H bending modes are as predicted by DFT calculations for a model with a  $\mu_2\text{SH}^-$  bridging the  $\text{Cu}_I\text{-Cu}_{IV}$  edge. The EPR spectrum of 1-hole  $\text{Cu}_Z$  indicates a ground state in which the spin is delocalized over 3 coppers in dominantly  $d_{x^2-y^2}$  orbitals. The absorption and MCD spectra show three  $\mu_4\text{S}^{2-}$  to Cu charge transfer transitions that have very similar energies to those observed for 1-hole  $\text{Cu}_Z^*$  (which has a hydroxide bridged  $\text{Cu}_I\text{-Cu}_{IV}$  edge) but a different intensity pattern, consistent with a change in spin distribution in the cluster from dominantly on  $\text{Cu}_I$  in 1-hole  $\text{Cu}_Z^*$  to more evenly delocalized over  $\text{Cu}_I$ ,  $\text{Cu}_{II}$ , and  $\text{Cu}_{IV}$ . This ground state spin distribution is consistent with that predicted from DFT calculations for the  $\mu_2\text{SH}^-$ . Based on the absence of a pH effect in 1-hole  $\text{Cu}_Z$  up to a pH of 10, the pKa of the edge thiolate in 1-hole  $\text{Cu}_Z$  is estimated to be 11–12.

The 2-hole state of  $\text{Cu}_Z$  was also spectroscopically defined, but no direct spectroscopic evidence for the protonation state of the edge ligand was obtained. DFT calculations of the deprotonation of a  $\mu_2\text{SH}^-$  ligand in 2-hole  $\text{Cu}_Z$  relative to 1-hole  $\text{Cu}_Z$  were used to determine that 2-hole  $\text{Cu}_Z$  likely has a sulfide edge ligand. Deprotonation of a  $\mu_2\text{SH}^-$  ligand in the 2-hole redox state is at least 12 kcal/mol more favorable than in the 1-hole redox state, after accounting for charge and dielectric effects. This yields a calculated pKa for a  $\mu_2\text{SH}^-$  ligand in 2-hole  $\text{Cu}_Z$  of 3 or less, which strongly suggests that 2-hole  $\text{Cu}_Z$  has an edge sulfide ligand at physiological pH. The calculated spectroscopic properties of a model of 2-hole  $\text{Cu}_Z$  with a  $\mu_2\text{S}^{2-}$  ligand are also consistent with those observed experimentally.

### 4.2 Similarities between 1-hole $\text{Cu}_Z$ and 1-hole $\text{Cu}_Z^*$

It has previously been observed that the spectral features of 1-hole  $\text{Cu}_Z$  are rather similar to those of 1-hole  $\text{Cu}_Z^*$ , despite the change in the nature of the edge ligand from a thiolate to a hydroxide.<sup>19, 28</sup> The spectroscopic similarities between 1-hole  $\text{Cu}_Z$  and 1-hole  $\text{Cu}_Z^*$  reflect similar bonding interactions between the  $\mu_4\text{S}^{2-}$  and the in plane coppers ( $\text{Cu}_I$ ,  $\text{Cu}_{II}$ , and  $\text{Cu}_{IV}$ ) which are not significantly perturbed by the nature of edge ligand. This results in similar transition energies in the absorption and MCD spectra, as the dominant transitions are due to  $\mu_4\text{S}^{2-}$  to Cu charge transfer, and a similar intense core  $\text{Cu-}\mu_4\text{S}^{2-}$  stretching mode

in the resonance Raman spectrum, observed at  $378\text{ cm}^{-1}$  in both sites. Small quantitative differences in the EPR hyperfine values and transition absorption and MCD intensities between the two sites arise from a perturbation of the spin density distribution of the cluster in 1-hole  $\text{Cu}_Z$ , where the more covalent  $\mu_2\text{SH}^-$  leads to delocalization of the spin on  $\text{Cu}_I$  (dominant in  $\text{Cu}_Z^*$ ) onto the edge  $\text{SH}^-$ . Despite the higher covalency of the  $\text{Cu}_Z$  site, the  $g$  values in the EPR spectra are similar for  $\text{Cu}_Z$  and  $\text{Cu}_Z^*$ , as the localization of spin on the four coordinate  $\text{Cu}_I$  in 1-hole  $\text{Cu}_Z^*$  leads to higher energy d-d transitions, opposing the decreased covalency, leading to the net low  $g$  values also observed experimentally for  $\text{Cu}_Z$ . The difference in edge ligation in the two sites is observed primarily in the resonance Raman enhanced vibrations, where a low energy  $\text{Cu}-\mu_2\text{SH}^-$  stretch at  $203\text{ cm}^{-1}$  and higher energy S-H bending modes at  $450$  and  $492\text{ cm}^{-1}$  are additionally enhanced in the dominant  $\mu_4\text{S}^{2-}$  to Cu CT transition in  $\text{Cu}_Z$  but not  $\text{Cu}_Z^*$ , due to the more covalent interaction between the coppers and the edge  $\text{SH}^-$ . Thus, the spectral similarities between 1-hole  $\text{Cu}_Z$  and 1-hole  $\text{Cu}_Z^*$  reflect similar bonding with the  $\mu_4\text{S}^{2-}$  ligand and the distribution of spin over  $\text{Cu}_I$ ,  $\text{Cu}_{II}$ , and  $\text{Cu}_{IV}$ . The differences in the vibrational spectra of the two sites reflect the  $\mu_2\text{SH}^-$  versus  $\mu_2\text{OH}^-$  edge ligation.

### 4.3 Insights into reactivity of 1-hole and 2-hole $\text{Cu}_Z$

1-hole  $\text{Cu}_Z$  has been shown to perform a slow 2 electron reduction of  $\text{N}_2\text{O}$  under single turnover conditions, with oxidation of both 1-hole  $\text{Cu}_Z$  and reduced  $\text{Cu}_A$  to generate resting 2-hole  $\text{Cu}_Z$  and 1 electron oxidized  $\text{Cu}_A$ .<sup>26</sup> A structure of  $P_3\text{N}_2\text{OR}$  obtained from crystals pressurized with  $\text{N}_2\text{O}$  shows a linear  $\text{N}_2\text{O}$  molecule binding above the  $\text{Cu}_{IV}$ - $\text{Cu}_{II}$  edge of the  $\text{Cu}_Z$  cluster (Figure 9).<sup>14</sup> The O of  $\text{N}_2\text{O}$  is thought to be oriented towards a solvent filled cavity between  $\text{Cu}_Z$  and  $\text{Cu}_A$ , where there is a hydrogen bonding interaction with a localized solvent molecule, while the N end of the molecule is  $2.8\text{ \AA}$  from  $\text{Cu}_{IV}$  and  $3.5\text{ \AA}$  from the  $\mu_2\text{SH}^-$  ligand. The spectroscopically and computationally defined protonation states for 1-hole and 2-hole  $\text{Cu}_Z$  indicate that the 1-hole  $\text{Cu}_Z$  site will donate both an electron and a proton upon oxidation, due to the significantly decreased  $\text{pK}_a$  of the  $\mu_2\text{SH}^-$  in the 2-hole redox state. The participation of a proton in the reduction of  $\text{N}_2\text{O}$  by 1-hole  $\text{Cu}_Z$  avoids the thermodynamically unfavorable 1-electron reduction of  $\text{N}_2\text{O}$  to  $\text{N}_2\text{O}^-$ , which is endergonic by  $25.4\text{ kcal/mol}$ , while the proton-coupled reduction of  $\text{N}_2\text{O}$  to form  $\text{N}_2$  and a hydroxyl radical is exergonic by  $7.4\text{ kcal/mol}$ .<sup>40</sup> However, a substantial barrier exists for this process due to the fact that  $\text{N}_2\text{O}$  is not activated through direct interaction with  $\text{Cu}_Z$  (the rate of  $\text{N}_2\text{O}$  reduction by 1-hole  $\text{Cu}_Z$  is  $2 \times 10^{-4}\text{ s}^{-1}$ ).<sup>26</sup> Thus the  $\text{N}_2\text{O}$  may alternatively be oriented with the O atom pointed towards  $\text{Cu}_Z$ , where it can directly accept a proton and an electron from the  $\mu_2\text{SH}^-$  to break the N-O bond and generate resting 2-hole  $\text{Cu}_Z$ , with transfer of the second electron from  $\text{Cu}_A$ . Since no intermediate is observed in the reduction of  $\text{N}_2\text{O}$  by 1-hole  $\text{Cu}_Z$ ,<sup>26</sup> the hydroxide product that would be formed after N-O bond cleavage would likely be rapidly protonated and released into the nearby solvent-filled cavity, rather than coordinating to the  $\text{Cu}_Z$  cluster.

The 2-hole resting state of  $\text{Cu}_Z$  has been defined as having a highly covalent sulfide ligand bridging the  $\text{Cu}_I$ - $\text{Cu}_{IV}$  edge. This resting species is potentially the starting point for the chemical conversion of  $\text{Cu}_Z$  to  $\text{Cu}_Z^*$ , the reactive form of the cluster for  $\text{N}_2\text{O}$  reduction.<sup>26</sup> *In vitro*, the presence of  $\text{O}_2$  is thought to promote the conversion of  $\text{Cu}_Z$  to  $\text{Cu}_Z^*$ , as isolation

of N<sub>2</sub>OR in the presence of O<sub>2</sub> results in samples with a high proportion of resting 1-hole Cu<sub>Z</sub><sup>\*</sup>, while the resting 2-hole state of Cu<sub>Z</sub> is obtained when the purification is performed in the absence of oxygen.<sup>16</sup> DFT calculations on the μ<sub>2</sub>S<sup>2-</sup> model of 2-hole Cu<sub>Z</sub> suggest that there are frontier molecular orbitals (FMOs) available to interact with O<sub>2</sub>. The α and β HOMOs of 2-hole Cu<sub>Z</sub> are occupied μ<sub>2</sub>S<sup>2-</sup> orbitals with dominant S p<sub>z</sub>' character (50% and 66% μ<sub>2</sub>S<sup>2-</sup> respectively, Figure 8). This μ<sub>2</sub>S<sup>2-</sup> p<sub>z</sub>' orbital is oriented perpendicular to the Cu<sub>3</sub>S<sub>2</sub> plane, towards the solvent-filled cavity where N<sub>2</sub>O, and by analogy O<sub>2</sub>, would access the Cu<sub>Z</sub> cluster. Based on these FMOs, reaction of the Cu<sub>Z</sub> site with O<sub>2</sub> would proceed via oxidation of the edge sulfide, rather than by a Cu-based oxidation. Since this is a four electron process, there will in principle also be electrons available from the sulfide for the reduction of the copper site, dependent on the nature of the oxidized sulfur product. However, it is unlikely that this is the mechanism involved in interconversion of Cu<sub>Z</sub> and Cu<sub>Z</sub><sup>\*</sup> *in vivo*, since resting Cu<sub>Z</sub><sup>\*</sup> has been isolated under exclusion of oxygen conditions from anaerobically grown cells in bacterial strains with accessory genes knocked-out.<sup>41</sup> Thus, the *in vivo* mechanism for interconversion of Cu<sub>Z</sub> and Cu<sub>Z</sub><sup>\*</sup>, which is required to maintain N<sub>2</sub>OR in the reactive Cu<sub>Z</sub><sup>\*</sup> form, and the role of accessory proteins in this process, remain to be identified.

## 5. Conclusions

We have used a combination of spectroscopies and DFT calculations to determine the protonation states of the edge sulfur in the 1-hole and 2-hole redox states of Cu<sub>Z</sub>. From resonance Raman spectroscopy, 1-hole Cu<sub>Z</sub> has a μ<sub>2</sub> thiolate ligand with a pK<sub>a</sub> of 11–12, due to the presence of S-H bending modes that are not perturbed up to pH 10. DFT calculations of a 1-hole cluster with a μ<sub>2</sub>SH<sup>-</sup> ligand reproduce the key spectral features of 1-hole Cu<sub>Z</sub>. The computational modeling of the 2-hole Cu<sub>Z</sub> site indicates that the edge ligand is a μ<sub>2</sub>S<sup>2-</sup> with a pK<sub>a</sub> of 3 or less, which is consistent with the absorption and resonance Raman features of 2-hole Cu<sub>Z</sub>. The nature of this edge ligand has been used to obtain insight into the slow reduction of N<sub>2</sub>O by 1-hole Cu<sub>Z</sub> and suggest how 2-hole Cu<sub>Z</sub> might react with O<sub>2</sub>, a possible route for the conversion of Cu<sub>Z</sub> to Cu<sub>Z</sub><sup>\*</sup> *in vitro*.

## Supplementary Material

Refer to Web version on PubMed Central for supplementary material.

## Acknowledgments

The authors acknowledge support of this research from the National Institutes of Health (R01DK031450 from the National Institute of Diabetes and Digestive and Kidney Diseases to E.I.S.) and National funds by FCT (Fundação para a Ciência e a Tecnologia) under the project PTDC/QUI-BIQ/116481/2010 (I.M.). The content is solely the responsibility of the authors and does not necessarily represent the official views of the National Institutes of Health.

## Notes and references

1. Tavares P, Pereira AS, Moura JGG, Moura I. Journal of Inorganic Biochemistry. 2006; 100:2087–2100. [PubMed: 17070915]
2. Thomson AJ, Giannopoulos G, Pretty J, Baggs EM, Richardson DJ. Philosophical Transactions of the Royal Society B-Biological Sciences. 2012; 367:1157–1168.

3. Zumft WG, Kroneck PMH. *Advances in Microbial Physiology*. 2007; 52:107–227. [PubMed: 17027372]
4. Bates, B.; Kundzewicz, ZW.; Wu, S.; Arnell, N.; Burkett, V.; Döll, P.; Gwary, D.; Hanson, C.; Heij, B.; Jiménez, B.; Kaser, G.; Kitoh, A.; Kovats, S.; Kumar, P.; Magadza, C.; Martino, D.; Mata, L.J.; Medany, M.; Miller, K.; Oki, T.; Osman, B.; Palutikof, J.; Prowse, T.; Pulwarty, R.; Räisänen, J.; Renwick, J.; Tubiello, F.; Wood, R.; Zhao, Z-C.; Arblaster, J.; Betts, R.; Dai, A.; Milly, C.; Mortsch, L.; Nurse, L.; Payne, R.; Pinskiwar, I.; Wilbanks, T., editors. *I. Secretariat*. 2008.
5. Richardson D, Felgate H, Watmough N, Thomson A, Baggs E. *Trends in Biotechnology*. 2009; 27:388–397. [PubMed: 19497629]
6. Ravishankara AR, Daniel JS, Portmann RW. *Science*. 2009; 326:123–125. [PubMed: 19713491]
7. Butterbach-Bahl K, Baggs EM, Dannenmann M, Kiese R, Zechmeister-Boltenstern S. *Philosophical Transactions of the Royal Society B-Biological Sciences*. 2013:368.
8. Bergaust L, Mao YJ, Bakken LR, Frostegard A. *Applied and Environmental Microbiology*. 2010; 76:8285–8285.
9. Bakken LR, Bergaust L, Liu BB, Frostegard A. *Philosophical Transactions of the Royal Society B-Biological Sciences*. 2012; 367:1226–1234.
10. Saleh-Lakha S, Shannon KE, Henderson SL, Zebarth BJ, Burton DL, Goyer C, Trevors JT. *Applied and Environmental Microbiology*. 2009; 75:5082–5087. [PubMed: 19525277]
11. Sorensen J, Tiedje JM, Firestone RB. *Applied and Environmental Microbiology*. 1980; 39:105–108. [PubMed: 6766699]
12. Morley N, Baggs EM. *Soil Biology & Biochemistry*. 2010; 42:1864–1871.
13. Brown K, Djinicovic-Carugo K, Haltia T, Cabrito I, Saraste M, Moura JGG, Moura I, Tegoni M, Cambillau C. *Journal of Biological Chemistry*. 2000; 275:41133–41136. [PubMed: 11024061]
14. Pomowski A, Zumft WG, Kroneck PMH, Einsle O. *Nature*. 2011; 477:234–U143. [PubMed: 21841804]
15. Ghosh S, Gorelsky SI, George SD, Chan JM, Cabrito I, Dooley DM, Moura JGG, Moura I, Solomon EI. *Journal of the American Chemical Society*. 2007; 129:3955–3965. [PubMed: 17352474]
16. Zumft WG, Coyle CL, Frunzke K. *Febs Letters*. 1985; 183:240–244.
17. Dell'Acqua S, Pauleta SR, Moura JGG, Moura I. *Philosophical Transactions of the Royal Society B-Biological Sciences*. 2012; 367:1204–1212.
18. Prudencio M, Pereira AS, Tavares P, Besson S, Cabrito I, Brown K, Samyn B, Devreese B, Van Beeumen J, Rusnak F, Fauque G, Moura JGG, Tegoni M, Cambillau C, Moura I. *Biochemistry*. 2000; 39:3899–3907. [PubMed: 10747777]
19. Rasmussen T, Berks BC, Butt JN, Thomson AJ. *Biochemical Journal*. 2002; 364:807–815. [PubMed: 12049645]
20. Solomon EI, Heppner DE, Johnston EM, Ginsbach JW, Cirera J, Qayyum M, Kieber-Emmons MT, Kjaergaard CH, Hadt RG, Tian L. *Chemical Reviews*. 2014; 114:3659–3853. [PubMed: 24588098]
21. Wuest A, Schneider L, Pomowski A, Zumft WG, Kroneck PMH, Einsle O. *Biological Chemistry*. 2012; 393:1067–1077. [PubMed: 23096349]
22. Pauleta SR, Dell'Acqua S, Moura I. *Coordination Chemistry Reviews*. 2013; 257:332–349.
23. Coyle CL, Zumft WG, Kroneck PMH, Korner H, Jakob W. *European Journal of Biochemistry*. 1985; 153:459–467. [PubMed: 3000778]
24. Ghosh S, Gorelsky SI, Chen P, Cabrito I, Moura JGG, Moura I, Solomon EI. *Journal of the American Chemical Society*. 2003; 125:15708–15709. [PubMed: 14677937]
25. Chan JM, Bollinger JA, Grewell CL, Dooley DM. *Journal of the American Chemical Society*. 2004; 126:3030–3031. [PubMed: 15012115]
26. Johnston EM, Dell'Acqua S, Ramos S, Pauleta SR, Moura I, Solomon EI. *Journal of the American Chemical Society*. 2014; 136:614–617. [PubMed: 24364717]
27. Rasmussen T, Berks BC, Sanders-Loehr J, Dooley DM, Zumft WG, Thomson AJ. *Biochemistry*. 2000; 39:12753–12756. [PubMed: 11041839]

28. Alvarez ML, Ai JY, Zumft W, Sanders-Loehr J, Dooley DM. *Journal of the American Chemical Society*. 2001; 123:576–587. [PubMed: 11456570]
29. Oganessian VS, Rasmussen T, Fairhurst S, Thomson AJ. *Dalton Transactions*. 2004:996–1002. [PubMed: 15252678]
30. Rasmussen T, Berks BC, Thomson AJ. *Journal of Inorganic Biochemistry*. 2001; 86:393–393.
31. Farrar JA, Thomson AJ, Cheesman MR, Dooley DM, Zumft WG. *Febs Letters*. 1991; 294:11–15. [PubMed: 1660405]
32. Farrar JA, Zumft WG, Thomson AJ. *Proceedings of the National Academy of Sciences of the United States of America*. 1998; 95:9891–9896. [PubMed: 9707571]
33. Antholine WE, Kroneck PMH, Zumft WG. *Molecular Physics*. 1998; 95:1247–1253.
34. Frisch, MJ.; Trucks, GW.; Schlegel, HB.; Scuseria, GE.; Robb, MA.; Cheeseman, JR.; Scalmani, G.; Barone, V.; Mennucci, B.; Petersson, GA.; Nakatsuji, H.; Caricato, M.; Li, X.; Hratchian, HP.; Izmaylov, AF.; Bloino, J.; Zheng, G.; Sonnenberg, JL.; Hada, M.; Ehara, M.; Toyota, K.; Fukuda, R.; Hasegawa, J.; Ishida, M.; Nakajima, T.; Honda, Y.; Kitao, O.; Nakai, H.; Vreven, T.; Montgomery, JA., Jr; Peralta, JE.; Ogliaro, F.; Bearpark, MJ.; Heyd, J.; Brothers, EN.; Kudin, KN.; Staroverov, VN.; Kobayashi, R.; Normand, J.; Raghavachari, K.; Rendell, AP.; Burant, JC.; Iyengar, SS.; Tomasi, J.; Cossi, M.; Rega, N.; Millam, NJ.; Klene, M.; Knox, JE.; Cross, JB.; Bakken, V.; Adamo, C.; Jaramillo, J.; Gomperts, R.; Stratmann, RE.; Yazyev, O.; Austin, AJ.; Cammi, R.; Pomelli, C.; Ochterski, JW.; Martin, RL.; Morokuma, K.; Zakrzewski, VG.; Voth, GA.; Salvador, P.; Dannenberg, JJ.; Dapprich, S.; Daniels, AD.; Farkas, Ö.; Foresman, JB.; Ortiz, JV.; Cioslowski, J.; Fox, DJ. *Gaussian, Inc; Wallingford, CT, USA*: 2009.
35. Chen P, Cabrito I, Moura JGG, Moura I, Solomon EI. *Journal of the American Chemical Society*. 2002; 124:10497–10507. [PubMed: 12197752]
36. Chen P, George SD, Cabrito I, Antholine WE, Moura JGG, Moura I, Hedman B, Hodgson KO, Solomon EI. *Journal of the American Chemical Society*. 2002; 124:744–745. [PubMed: 11817937]
37. Pomowski A, Zumft WG, Kroneck PMH, Einsle O. *Acta Crystallographica Section F-Structural Biology and Crystallization Communications*. 2010; 66:1541–1543.
38. Bar-Nahum I, Gupta AK, Huber SM, Ertem MZ, Cramer CJ, Tolman WB. *Journal of the American Chemical Society*. 2009; 131:2812. [PubMed: 19206272]
39. Noyes RM. *Journal of the American Chemical Society*. 1962; 84:513.
40. Koppenol WH. *Free Radical Biology and Medicine*. 1991; 10:85–87. [PubMed: 1646753]
41. Wunsch P, Korner H, Neese F, van Spanning RJM, Kroneck PMH, Zumft WG. *Febs Letters*. 2005; 579:4605–4609. [PubMed: 16087179]

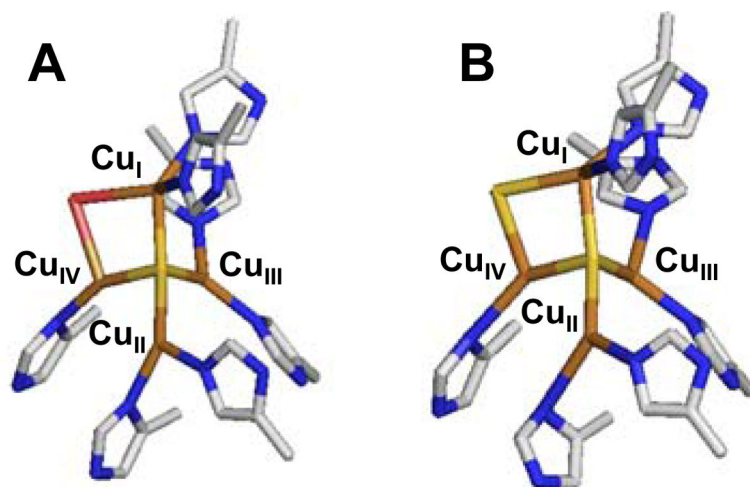


**Figure 1.** The two forms of the tetranuclear copper sulfide active site of nitrous oxide reductase. A)  $\text{Cu}_2^*$  in *PdN}\_2\text{OR}* isolated aerobically (PDB ID 1FWX).<sup>13</sup> B)  $\text{Cu}_2$  in *PsN}\_2\text{OR}* isolated anaerobically (PDB ID 3SBP).<sup>14</sup>



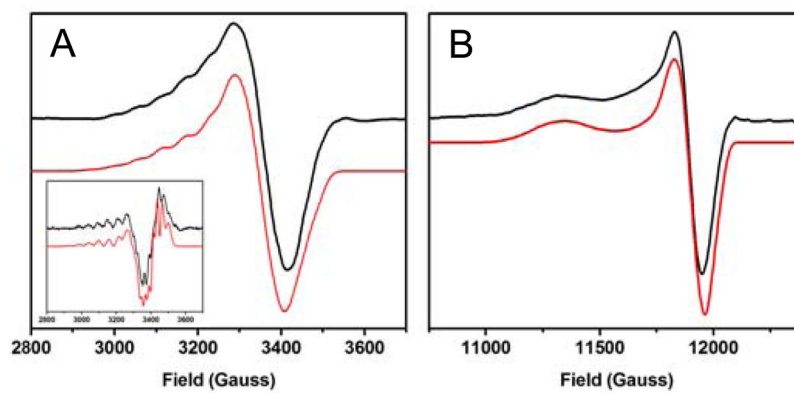


**Figure 2.** EPR spectra of 1-hole Cu<sub>Z</sub> (black) with simulations (red). A) X-band at 77 K, 9.6349 GHz. Inset: 2<sup>nd</sup> derivative of the X-band. B) Q-band at 77 K, 34.082 GHz.

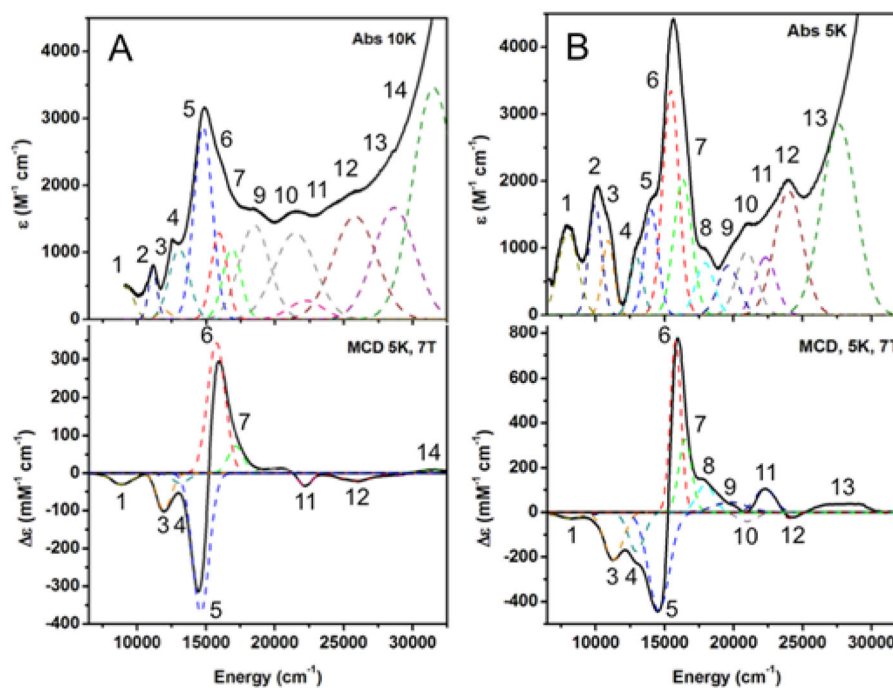


**Figure 3.**

Low temperature absorption and MCD spectra of A) 1-hole  $\text{Cu}_Z$ , 10 K absorption, 5 K and 7 T MCD. B) 1-hole  $\text{Cu}_Z^*$ , 5 K absorption, 5 K and 7 T MCD (adapted from Ref. <sup>15</sup>).

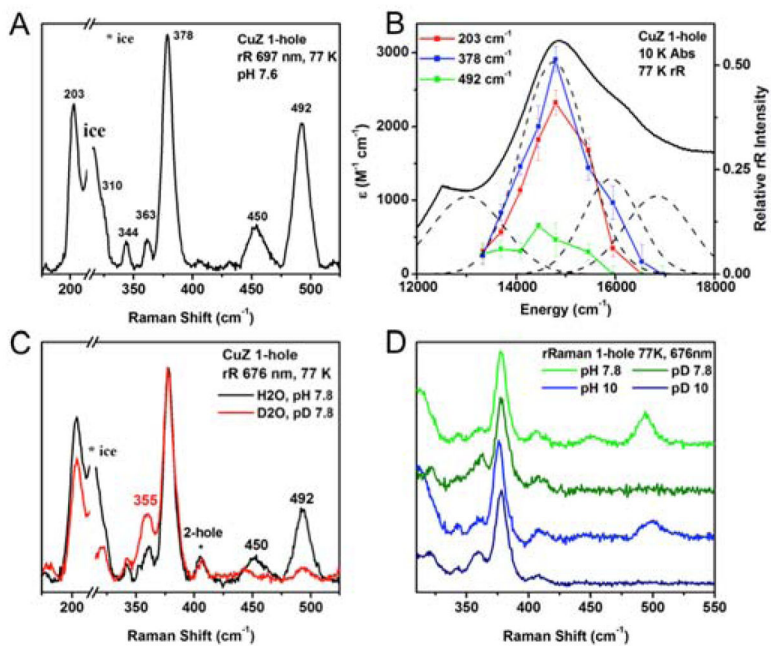


**Figure 4.**

A) Resonance Raman spectrum of 1-hole Cu<sub>Z</sub> at 77 K, excitation energy 697 nm. B) Excitation profile of the 203, 378, and 492 cm<sup>-1</sup> vibrations. C) H-D isotope shift of the vibrations of 1-hole Cu<sub>Z</sub>, performed in pH or pD 7.8 100 mM phosphate, excitation energy 676 nm. D) Comparison of SH bending vibrations at pH/pD 7.8 (green) and pH/pD 10 (blue).

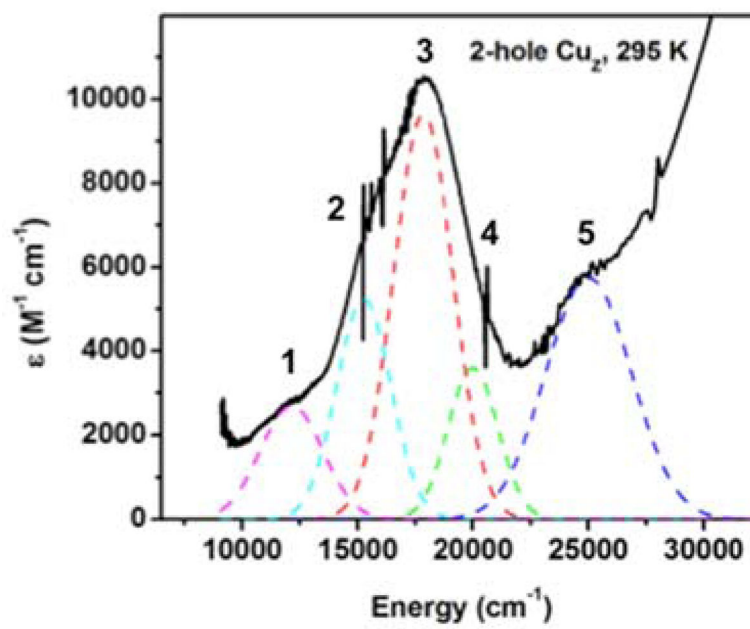


**Figure 5.** Absorption spectrum of 2-hole  $\text{Cu}_Z$  at room temperature, obtained after ascorbate reduction of  $\text{Cu}_A$  and subtraction of spectral contribution of 1-hole  $\text{Cu}_Z^*$ .

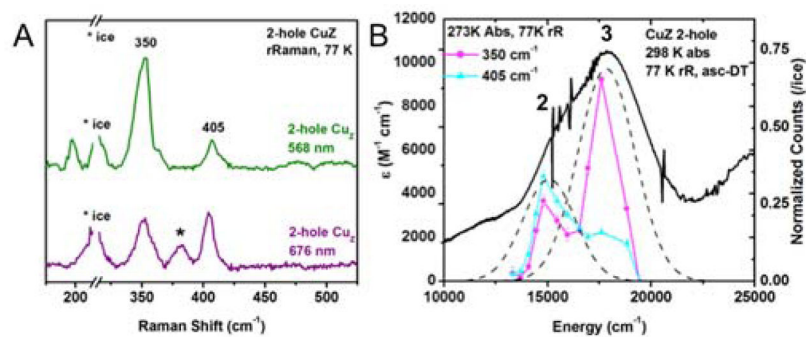


**Figure 6.**

A) Resonance Raman spectra of 2-hole CuZ at 77 K and two excitation energies, 568 nm (green) and 676 nm (purple). Starred vibration is due to 1-hole CuZ\*. B) Excitation profiles of the 350 and 405 cm<sup>-1</sup> vibrations overlaid with the room temperature absorption spectrum.

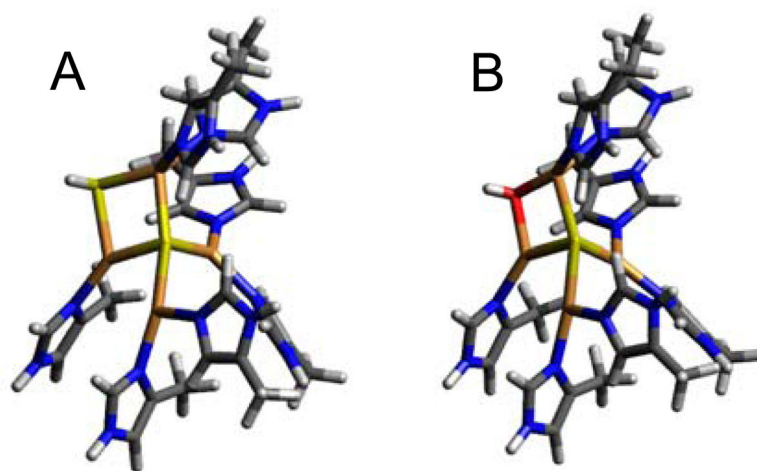


**Figure 7.** Computational models of A) 1-hole Cu<sub>2</sub> and B) 1-hole Cu<sub>2</sub>\* (B3LYP, TZVP on Cu, S, and ligating N atoms, and SV on all remaining atoms, PCM of 4.0).

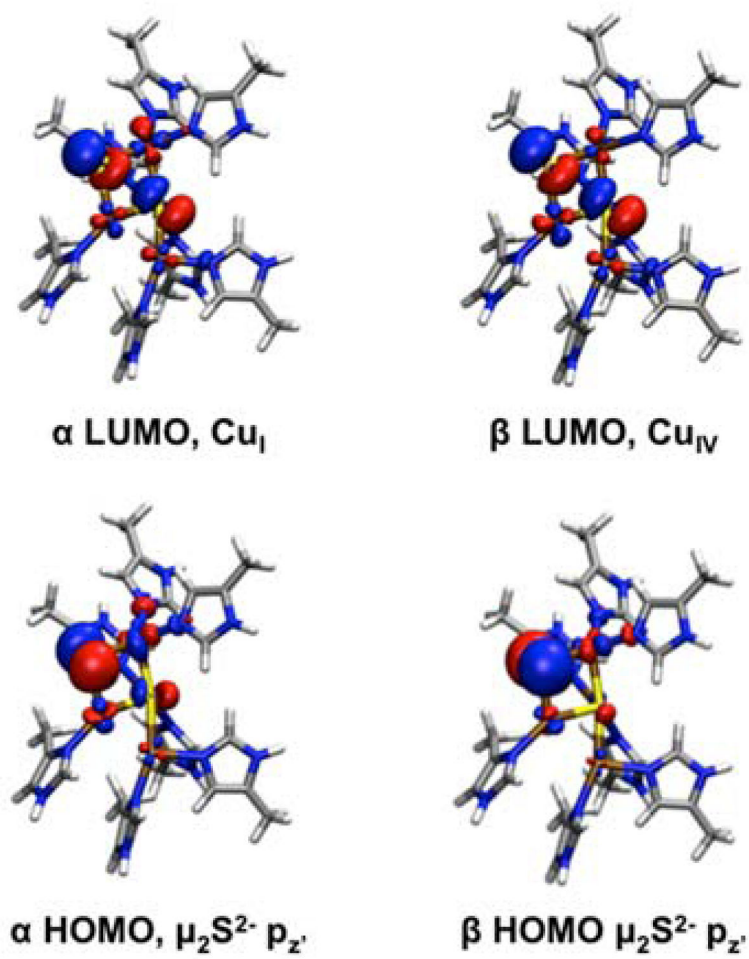


**Figure 8.** Frontier molecular orbitals of 2-hole Cu<sub>2</sub> (two sulfide model).

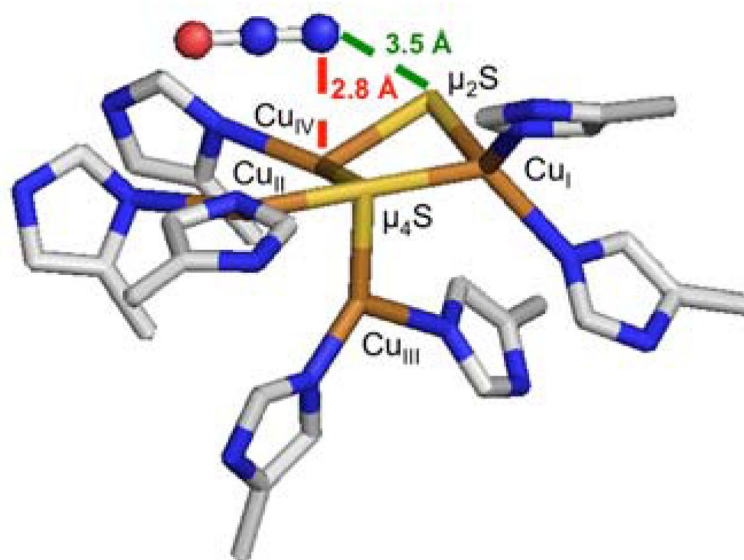


**Figure 9.** Crystal structure of N<sub>2</sub>O bound to Cu<sub>2</sub> (PDB ID: 3SBR, subunit C, resolution 1.7 Å).<sup>14</sup>



**Table 1**

EPR  $g$  and  $A$  values for 1-hole  $\text{Cu}_Z$ , obtained from simulations included in Figure 2 and Figure S2 with values for  $\text{Cu}_Z^*$  reproduced from Reference <sup>15</sup>.

	1-hole $\text{Cu}_Z$	1-hole $\text{Cu}_Z^*$
$g_{\parallel}$	2.152	2.160
$A_{\parallel}$	$56 \times 10^{-4} \text{ cm}^{-1}$	$61 \times 10^{-4} \text{ cm}^{-1}$
	$56 \times 10^{-4} \text{ cm}^{-1}$	$23 \times 10^{-4} \text{ cm}^{-1}$
	$56 \times 10^{-4} \text{ cm}^{-1}$	
$g_{\perp}$	2.042	2.043
$A_{\perp}$	$20 \times 10^{-4} \text{ cm}^{-1}$	$25 \times 10^{-4} \text{ cm}^{-1}$
	$20 \times 10^{-4} \text{ cm}^{-1}$	$20 \times 10^{-4} \text{ cm}^{-1}$
	$20 \times 10^{-4} \text{ cm}^{-1}$	

**Table 2**

Mulliken atomic spin density of 1-hole computational models with SH<sup>-</sup> and OH<sup>-</sup> bridging ligands on the Cu<sub>I</sub>-Cu<sub>IV</sub> edge, with % Cu and % d orbital character in their ground state wavefunctions.

Edge Ligand	Mulliken Atomic Spin Density				
	Cu <sub>I</sub>	Cu <sub>II</sub>	Cu <sub>III</sub>	Cu <sub>IV</sub>	$\mu_2L^-$
SH <sup>-</sup> bridge	0.17	0.11	0.06	0.10	0.34
OH <sup>-</sup> bridge	0.26	0.09	0.04	0.13	0.31

**Table 3**

Mulliken spin densities on Cu and S atoms in the  $\alpha$  and  $\beta$  LUMOs of the broken symmetry singlet 2-hole  $\text{Cu}_4\text{S}(\text{SH})$  and  $\text{Cu}_4\text{S}_2$  models (B3LYP, TZVP on Cu, S, and ligating N atoms, and SV on all remaining atoms, PCM of 4.0).

	Mulliken Spin Density						$\mu_4\text{S}^{2-}$
	$\mu_2\text{L}$	$\text{Cu}_\text{I}$	$\text{Cu}_\text{II}$	$\text{Cu}_\text{III}$	$\text{Cu}_\text{IV}$		
2-hole SH <sup>-</sup> S=0	$\alpha$ LUMO	0.16	0.37	0.06	0.06	0.04	0.20
	$\beta$ LUMO	0.17	0.03	0.17	0.09	0.16	0.30
2-hole S <sup>2-</sup> S=0	$\alpha$ LUMO	0.33	0.22	0.06	0.04	0.07	0.23
	$\beta$ LUMO	0.37	0.05	0.06	0.05	0.14	0.27